

# DEVELOPMENT OF DAMAGE TOLERANT COMPOSITE LAMINATES USING ULTRA-THIN INTERLAMINAR ELECTROSPUN THERMOPLASTIC NANOFIBRES

Danning Li<sup>1</sup>, Raphael Prevost<sup>1</sup>, David Ayre<sup>1</sup>, Ata Yoosefinejad<sup>2</sup>, Saeid Lotfian<sup>1,3</sup>, Feargal Brennan<sup>3</sup>,  
Hamed Yazdani Nezhad<sup>1,\*</sup>

<sup>1</sup>Enhanced Composites & Structures Centre, School of Aerospace, Transport and Manufacturing,  
Cranfield University, MK43 0AL, UK

<sup>2</sup>Munro Technology Limited, Lufton Height Commerce Park, Yeovil, BA22 8UY, UK

<sup>3</sup>Naval Architecture, Ocean & Marine Engineering, University of Strathclyde, G1 1XQ, UK

\*Corresponding author: [h.yazdani-nezhad@cranfield.ac.uk](mailto:h.yazdani-nezhad@cranfield.ac.uk), Web Page: <http://www.cranfield.ac.uk>

**Keywords:** polymer-matrix composite, interlaminar fracture toughness, nanofiber, electrospinning

## Abstract

Carbon fibre-reinforced polymer (CFRP) composites are extensively used in high performance transport and renewable energy structures. However, composite laminates face the recurrent problem of being prone to damage in dynamic and impact events due to extensive interlaminar delamination. Therefore, interlaminar tougheners such as thermoplastic veils are introduced between pre-impregnated composite plies or through-thickness reinforcement techniques such as tufting are employed. However, these reinforcements are additional steps in the process which will add a degree of complexity and time in preparing composite lay-ups.

A novel material and laying-up process is proposed in this paper that uses highly stretched electrospun thermoplastic nanofibers (TNF) that can enhance structural integrity with almost zero weight penalty (having 0.2gsm compared to the 300gsm CFRP plies), ensuring a smooth stress transfer through different layers, and serves directional property tailoring, with no interference with geometric features e.g. thickness.

Aerospace grade pre-impregnated CFRP composite laminates have been modified with the TNFs (each layer having an average thickness of <1 micron) electrospun on each ply, and autoclave manufactured, and the effect of the nanofibers on the fracture toughness has been studied. Interlaminar fracture toughness specimens were manufactured for Mode I (double cantilever beam) and Mode II (end notched flexural) fracture tests. Such thin low-density TNF layers added an improvement of 20% in failure loads and fracture toughness in modes I and II.

## 1. Introduction

Composite materials are extensively used in transport and renewable energy sectors due to their high mechanical properties and low density. The use of polymer-matrix composites (PMCs) on primary aircraft structures enables substantial fuel efficiency, and therefore have direct impact on CO<sub>2</sub> emission reduction.

One of the principal limitation of increasing use of PMC laminates in modern aircrafts (e.g. A350 and B787) is the low damage tolerance of these materials. In particular, delamination growth between reinforcing plies is considered one of the most predominant and life-limiting type of damage encountered in composite laminates during service that can be detrimental to flight safety [1-3]. Furthermore, while impact can significantly reduce mechanical properties, it is barely visible impact damage (BVID), hardly detectable by existing non-destructive inspections (NDI) techniques. 87% of total composite damage is caused by impact with energy ranging from 10 to 100 joules, as low-velocity (energy) impacts. In such terms, several different methods have been developed to toughen composite materials to resist interlaminar delamination. The crack propagation is quantified by the strain energy release rate ( $G$ ), which is the amount of energy needed to create a crack surface (J/m<sup>2</sup>), also known as the delamination toughness. Its value can vary depending on the crack length because of a phenomenon called fibre bridging [4-6].

D. Li, R. Prevost, D. Ayre, A. Yoosefinejad, S. Lotfian, F. Brennan, H. Yazdani Nezhad

Preventing delamination occurrence has to be taken into account during the design and conception of structures, sources of out-of-plane stressing being often caused by load-path discontinuity. Since manufacturing defects as well as impacts cannot be entirely avoided [7-9], a security factor has to be used which increases the weight of structures. Thus, increasing intrinsic fracture toughness of composite material is crucial. Interleaving techniques have been developed, by inserting ductile interlaminar layers with great shear strain and toughness between the original composite plies. This method is effective as it enables impact damage absorption and hinders the damage at its initial stage, however these inserted layers, although very tough, are also heavy and reduce the specific stiffness and specific strength of the laminates [10].

Interlaminar delamination develops at the interface between two adjacent laminas at low-velocities but leads to a significant drop in the structure's mechanical properties (e.g. contributing to 65% dissipation of impact energy according to [8]). It mainly occurs at interfaces between plies of different orientation, as these don't deform similarly and this deformation mismatch causes shear strains and ultimately de-cohesion. Delamination generally has an oblong or peanut shape, inclined towards the same direction as the fibre situated directly underneath. When many successive plies have the same orientation, the remaining mismatching interfaces will suffer from extensive damage, and the laminate damage resistance is reduced, while increasing the number of dissimilar interfaces increase the energy absorbed during delamination [11]. Generally speaking, that means that thicker plies would have less interfaces for the same structure's width and leads to less energy absorbed during delamination.

Interleaving techniques have shown encouraging results in terms of the laminate's fracture toughness enhancement. To tackle its main drawback, the weight penalty and addition to overall thickness, researchers have studied the possibility to introduce a light layer of thermoplastic electrospun nanofibers. Electrospinning is an established and scalable technique to generate continuous fibers in the nanoscale, with a broad range of constituents available. The fibers are produced from a polymeric solution, stretched by the electrostatic repulsion between surface charges and the evaporation of solvent [12]. Akangah et al. [13] have described the process to produce electrospun nanofibers.

In particular, interfacial toughening based on nanofibers electrospun from thermoplastics is of increasing interest [14-24]. The advantages of these approaches is that there is limited thickness or weight penalty, since the nanofibrous mat is very thin and highly localised between the plies interfaces, leading to only marginal loss of in-plane properties. Besides, the cost of nanofiber fabrication is limited and the composite process doesn't have to be entirely changed to make the composite benefit from the reinforcement.

The aim of this study is to develop and evaluate a new toughening technique based on the embedment of nanofibers within a composite material. The method should combine low added weight and limited degradation of overall mechanical properties, and enhance fracture toughness properties.

## **2. Materials and Manufacturing**

The prepreg used in this study is high performance aerospace grade (HexPly<sup>®</sup> M21), supplied by Hexcel, made of unidirectional (UD) Toray 800S intermediate modulus carbon fibres and pre-impregnated with a high performance tough epoxy matrix, M21, which was designed to exhibit excellent damage tolerance. Ply mass is 305gsm with nominal thickness of 0.26mm and 56.6% Vol.% carbon fibre. The tensile strength of the cured composite is 3039MPa and the modulus is 172GPa [25, 26].

Electrospinning was done by Munro Technology Limited, using their TNF product, FibroTend, consisting of highly stretched unidirectional nylon 6,6 nanofibers. The TNFs were directly electrospun on the surface of each composite prepreg ply as shown in Figure 1. The fragile nanofibers are then covered with a layer of waxed paper for protection. This protection also protects the material from absorbing the humidity contained in the air as the nylon is by nature hygroscopic.



Figure 1: FibroTend, nylon 6,6 TNFs directly electrospun deposited on the CFRP composite surface

The prepreg lamina received as a roll of 300mm width and was cut into rectangles of 200mm × 165mm and 350mm × 175mm for the plies with orientations in 0° or 90°. For the plies oriented at -45° or +45°, parallelograms of 550mm × 424mm were cut. Plies were carefully stacked and the waxed paper protecting the nanofibers was released in a protective environment just before laying up to avoid moisture absorption. Post CFRP laying-up, the specimens were cured using a vacuum bag in the autoclave according to Hexcel's datasheet [25], at 180°C and 7 bar for 120 minutes, with the initial heating rate of 1°C/min. Specimens were then cut by waterjet. The thickness was  $4.15 \pm 0.4$  mm close to the nominal 4.19 mm.

End blocks were manufactured to equip double cantilever (DCB) and end notched flexural (ENF) specimens for mode I testing. The specimens edges were polished for better adhesion with the end blocks before gluing, and clamps were used to fix the blocks and the specimens together during heating in an oven. The edge of the specimens were coated with a thin layer of typewriter correction fluid and ruler marks were drawn on their edge with a pencil to enable to follow the crack propagation.

### 3. Experiments

#### 3.1. Fracture toughness specimens and tests

Fracture toughness specimens for mode I followed the ASTM D5528 standard [27] using DCB specimens in 20mm × 125mm dimensions. For mode II, ASTM D7905 [28] was used for the ENF specimens in 20mm × 180mm. 16 plies per each category were stacked in 0° orientation as required by the standards, for a total thickness of 4.2mm. Edge side 50mm and 65mm length release films were introduced to the DCB and ENF specimens, respectively, to create pre-existing crack. Four specimens per category were manufactured to examine the repeatability of the test data. Reference specimens (i.e. without TNFs) were also manufactured for DCB and ENF testing. Fracture toughness tests were performed using a Zwick 10kN force machine, equipped with a load cell of 2.5 kN. The crosshead opening displacement speed for all the tests was set at 0.7 mm/minute to ensure quasi-static condition loading for all tests. Great care was taken to avoid initial loading when fitting the load blocks on the jigs, and to verify the pins inserted in the blocks were parallel so as to not introduce any torsional moment. Load and displacement data were recorded using the TestXpert v5.01 software on a PC. In both testing, the crack measurement was carried out optically via magnifying glass at every half centimetres after 5mm crack length was reached.

#### 3.2. Microscopy

Optical microscopy and SEM were used to identify damage mechanisms occurred in the specimens after fracture toughness tests. The specimens for SEM were coated with a thin plasma gold plasma layer, 15 nm thickness, to improve the imaging of specimens via discharging electrons off the specimens' surface.

## 4. Results and Discussion

### 4.1. Fracture toughness test data

The fracture toughness was obtained according to the ASTM recommendation based on the modified beam theory (equation 1), with correction for end blocks and large displacement (as the specimens'

crack was propagated longer than the minimum required). The distance between the hole and the back of the block, is equal to 4 mm, and  $L'$  the distance between the hole and the surface of the DCB, is equal to 3.5 mm. These values are the cause for the need of a correction and they have already been reduced to the minimal possible in the blocks' design.

$$G_I = \frac{3P\delta}{2b(a + \Delta)} \times \frac{F}{N} \quad (1)$$

where  $P$  is applied load,  $\delta$  is the load point displacement,  $b$  is the specimen's width, and  $a$  is the delamination crack length.  $\Delta$  is a correction factor that accounts for the fact that opening DCB is not a perfect cantilever with its end totally fixed. It could be determined experimentally by generating a least squares plot of the cube root of compliance,  $C^{1/3}$ , as a function of delamination length. The large displacement factor,  $F$  in equation (1) corrects the fact that as the angle of the end blocks changes during loading, their orientation also changes and influence the distance between the crack front and the loading pin. The use of end blocks, that can cause a stiffening effect of the specimen arms, or different displacement relative to the ideal loading point, is corrected by the  $N$  factor.  $F$  and  $N$  are given by:

$$F = 1 - \frac{3}{10} \left(\frac{\delta}{a}\right)^2 - \frac{3}{2} \left(\frac{\delta t}{a^2}\right) \quad (2)$$

$$N = 1 - \left(\frac{L'}{a}\right)^3 - \frac{9}{8} \left[1 - \left(\frac{L'}{a}\right)^2\right] \left(\frac{\delta t}{a^2}\right) - \frac{9}{35} \left(\frac{\delta}{a}\right)^2 \quad (3)$$

Load-displacement curves are shown in Figure 2 from which the evolution of fracture toughness with the crack length propagation has been extracted according to equations (1-3) (Figure 3). FT is denoted by the TNF-FibroTend material in the two figures.

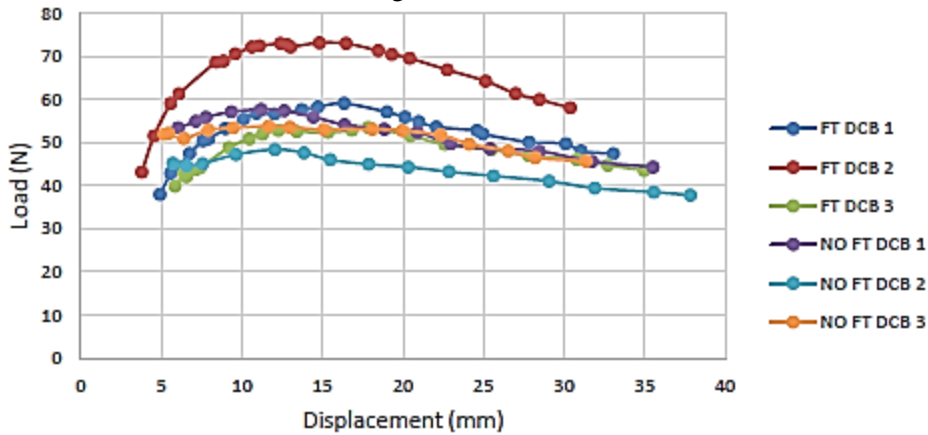


Figure 2: Comparison of load-displacement curves for DCB specimens with and without the TNFs

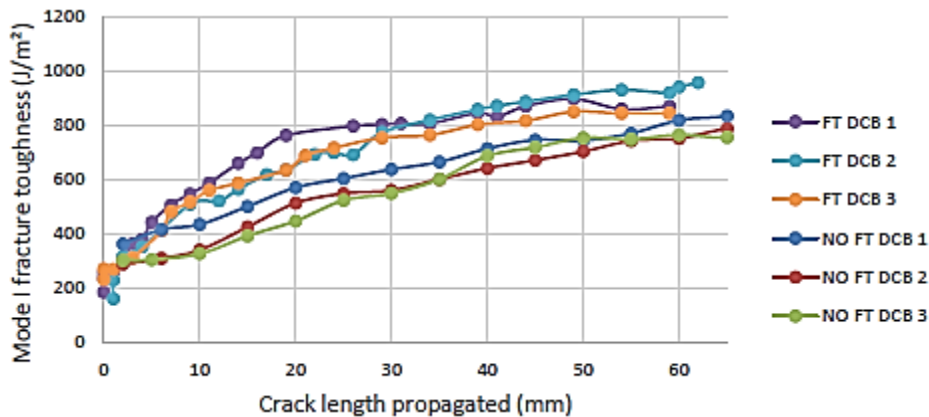


Figure 3: Evolution of fracture toughness in opening mode with delamination crack length in DCB specimens with and without TNFs

The average plots for the DCB specimens, with or without FibroTend, are shown in Figure 4 and Figure 5, with  $\pm 1.645$  specimen's standard deviation. It could be seen that the relatively high scatter in the load-displacement data has not equally mapped to the fracture toughness data as the high value seen on FT DCB 2 is corrected by the fracture toughness calculations.

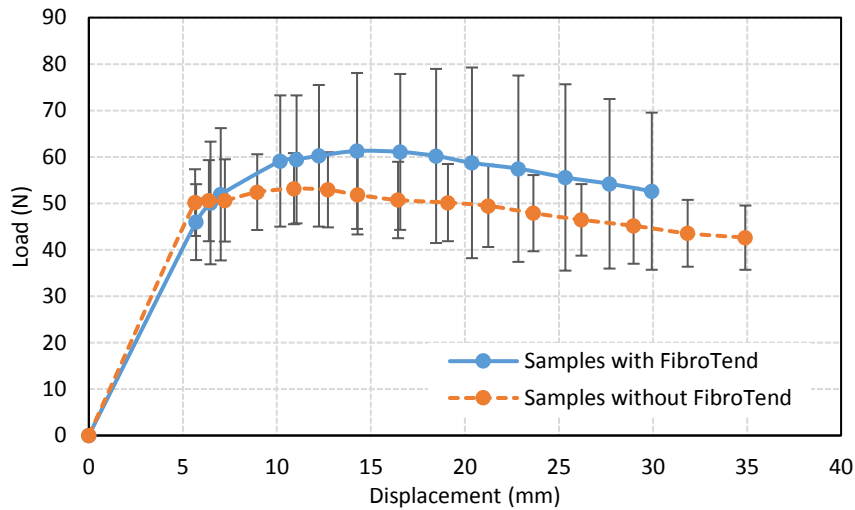


Figure 4: Averaged load-displacement data for DCB specimens

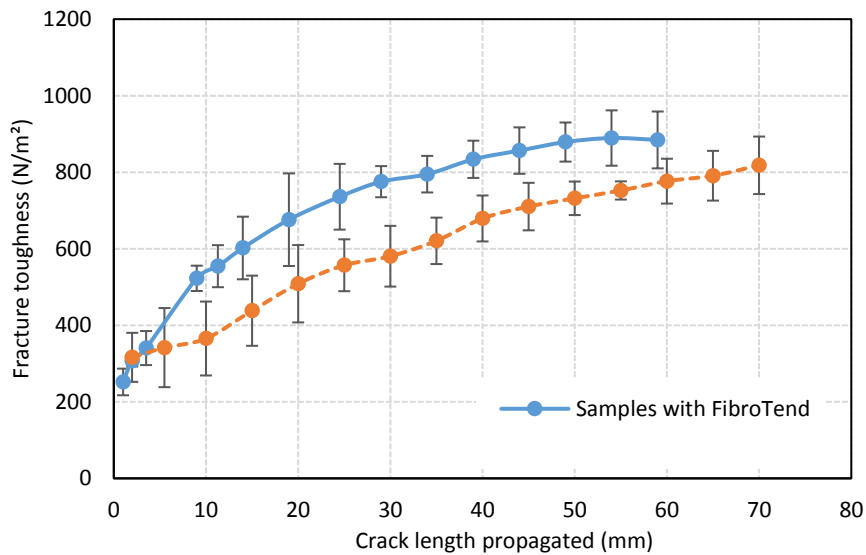


Figure 5: Averaged fracture toughness data for DCB specimens

The high dispersion (represented by the standard deviation) observed in the load-displacement plot for DCB specimen, particularly with FibroTend, is attributed to one particular specimen tested at a higher load (FT DCB2 in Figure 2). Accounting for correction factors in fracture toughness calculations, much fracture toughness data obtained are low-scattered and reliable.

The specimens with the TNFs exhibited high fiber bridging phenomenon (shown in Figure 6), evidenced by the increase in fracture toughness data in Figure 5 in the state of crack propagation, and by the increase in load even after the elastic zone. This fiber bridging difference could be due to the nylon TNFs sticking to the carbon fibers and the thermoset matrix of the composites and hindering full separation as postulated in [15]. The average maximum load increases from 53.1 N to 61.2 N, which represent 15% improvement. Comparing the fracture toughness data at 50mm-60mm crack length showed an increase from 752 J/m<sup>2</sup> to 890.2 J/m<sup>2</sup>, leading to 18% improvement.

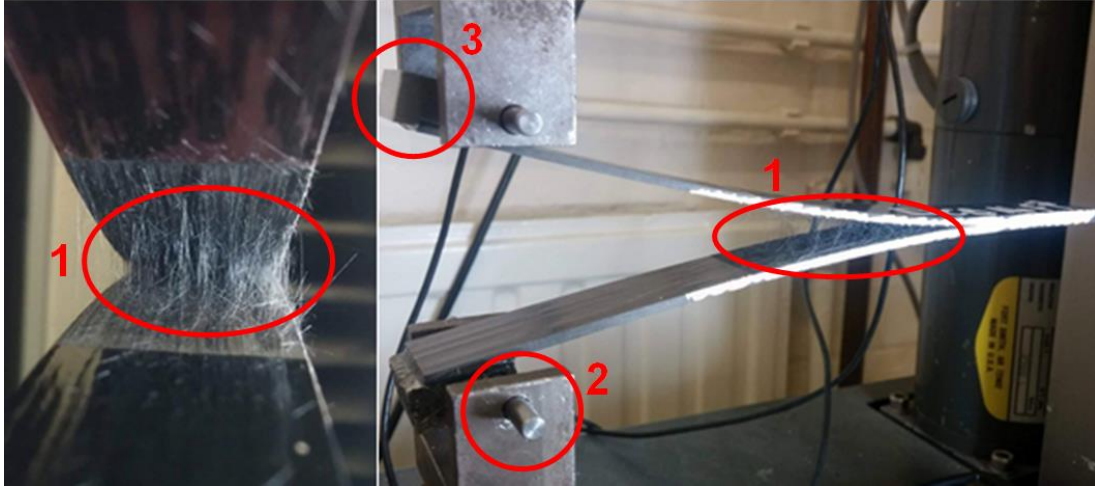


Figure 6: DCB specimen in a setup with pins (2) and end blocks (3): TNF fiber bridging in region (1)

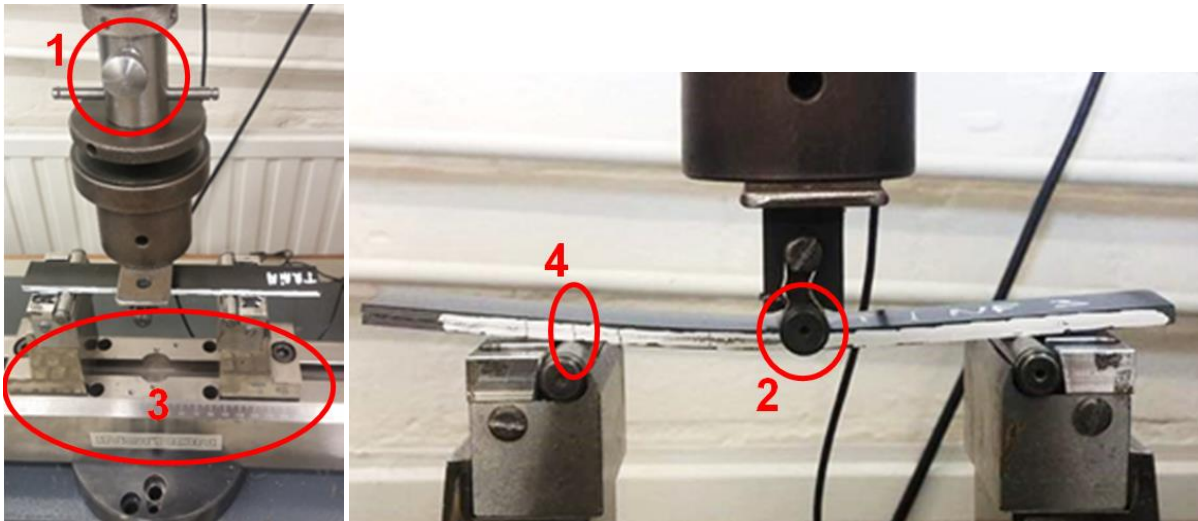


Figure 7: ENF setup with 2.5 kN load cell, adaptor (1), loading roller, and supporting jig (left). On the top right is an ENF specimen being tested, with the 30 mm mark (2) on the left supporting roller

The same procedure as the DCB specimens was followed to obtain data for the ENF ones (Figure 7). Each delamination propagation is accompanied by the two compliance calibration curves at 20mm and 40mm, and the unloading values. As the disparity in load-displacement data was relatively high, it was decided to calculate the mode II fracture toughness according to the modified expression in [29]:

$$G_{II} = \frac{9P_{max}^2 a_0^2}{16B^2 h^3 E_f} \quad (4)$$

where  $P_{max}$  is the maximum force reached during the fracture tests,  $B$  is the specimen width,  $a_0$  is the initial crack length (i.e. 30 mm),  $h$  is half of the total thickness of the specimens.  $E_f$  is the modified flexural modulus of the ENF specimen according to ASTM D790 [30], given by:

$$E_f = \frac{L^3 m}{4ABh^3} \quad (5)$$

where  $L$  is the half span of the test, 50mm in our case, and  $m$  is the slope of the tangent to the initial straight-line portion of the load-deflection curve of the test. The value of flexural modulus obtained was

very similar to the one from the ENF test. The flexural modulus found from the DCB test showed high disparity with strong dependence on the crack length, so they were discarded. The averaged data obtained from the compliance method and the modified expression (eq. (4)) are shown in Table 1.

Table 1: Summary of ENF test results

Specimen type	$P_{max}$ (N)	$E_f$ (GPa)	Standard, compliance based, $G_{II}$ (J/m <sup>2</sup> )	Modified, $E_f$ based, $G_{II}$ (J/m <sup>2</sup> )	Absolute difference
ENF with no TNF	594.8	69.6	700.7	702.8	47.2
ENF with TNF	818.0	92.8	819.4	904.7	130.5
Standard dev. (without TNF)	0.171	0.238	0.227	0.182	0.547
Standard dev. (with TNF)	0.116	0.117	0.176	0.210	1.674

Figure 8 shows the improvement in the ENF specimens taking up the maximum load in the presence of TNFs, and Figure 9 shows the effects on the improvement in mode II fracture toughness data. The confidence interval obtained from the error bars shown in the figures is 68.2%.

ENF tests had relatively high variation on load data. However, the fracture toughness results calculated from the ASTM standard's compliance calibration method gives as reliable data as the one obtained from the method based on the flexural modulus.

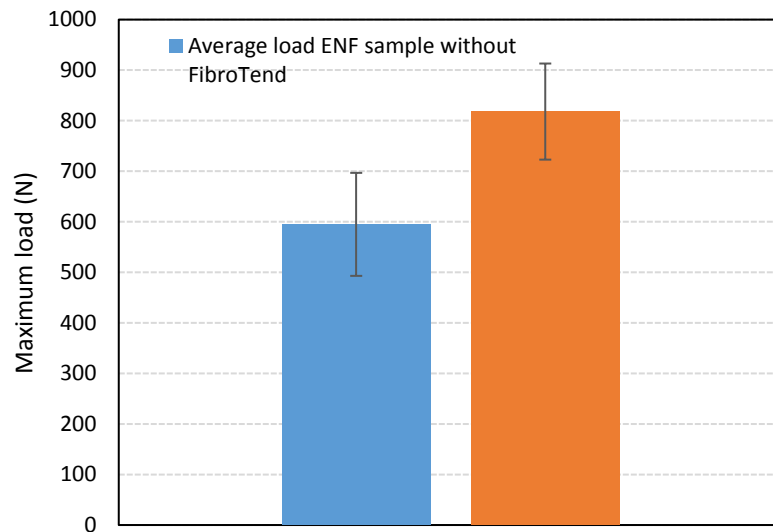


Figure 8: Comparison of maximum load data for ENF specimens with and without TNFs

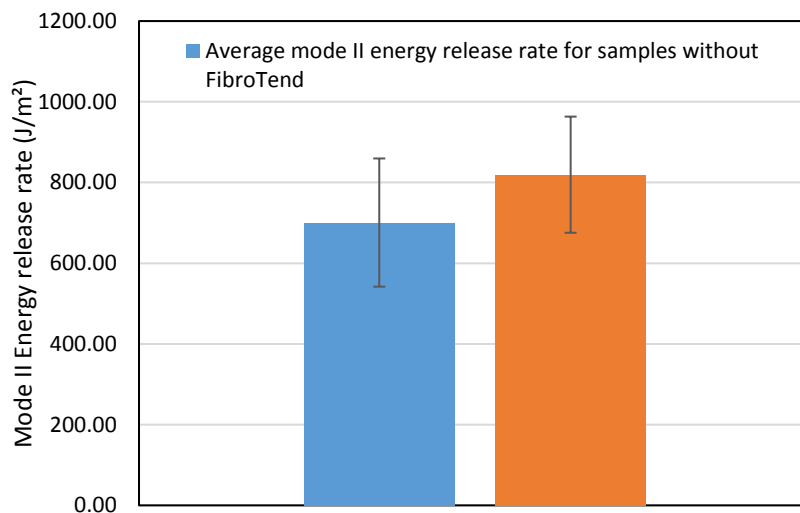


Figure 9: Comparison of mode II fracture toughness for ENF specimens with and without TNFs

## 4.2. Microscopy data

Fractured surfaces of the DCB specimens with and without the TNFs are shown in Figure 10. It is not possible to directly evidence the presence of the TNF layers. However, their effect on broken carbon fibers during fiber bridging and the damages matrix is observed. The matrix damage has exhibited more ductile failure with significantly more cup-shaped patterns in the DCB specimens with the TNFs. The effect on carbon breakage is trivial. Wettage of several carbons by the TNFs is evident, though no affirmation on the toughening effects can be made for fibre-matrix debonding.

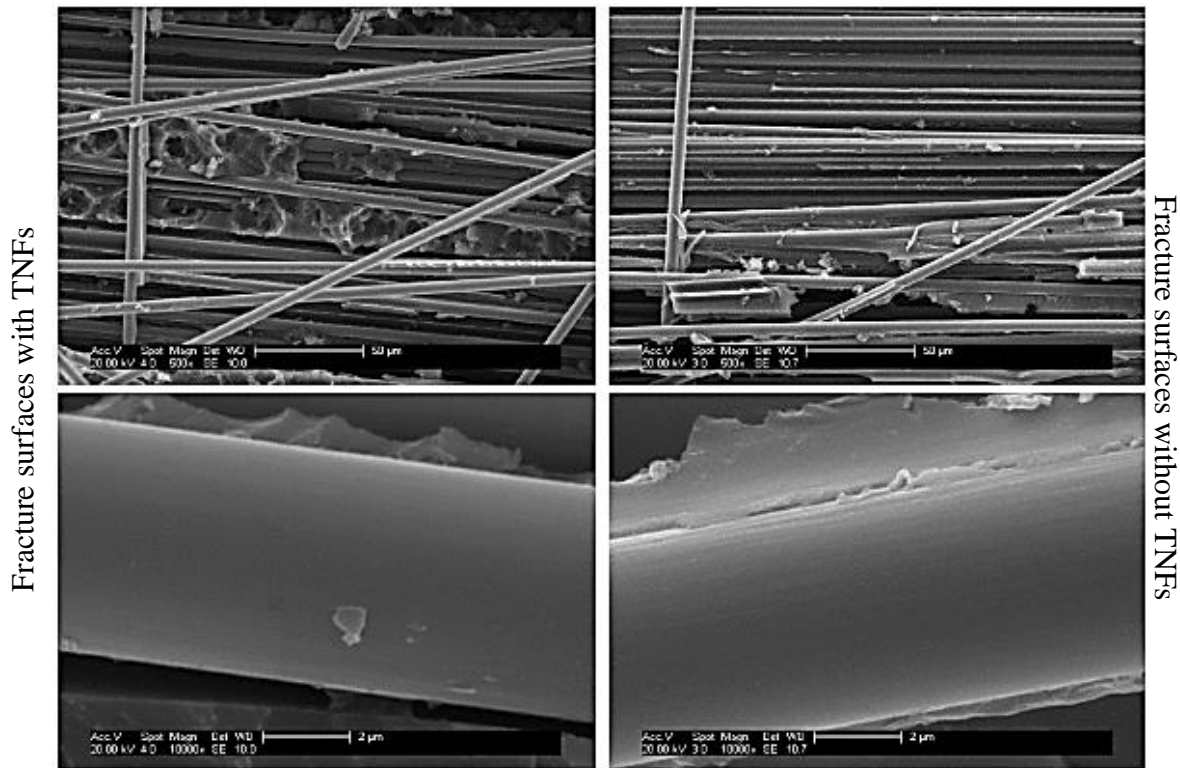


Figure 10: SEM images of DCB specimens at ultimate failure with and without TNFs

Neither optical microscopy nor SEM showed direct presence of the TNF after the cure. This is due to a very slight contrast between the composite's epoxy and the TNF microscopic data. The DCB and ENF data, however, has presented the TNF behaving as classical interleave at the concentration of 0.2 g/m<sup>2</sup>.

## 5. Conclusions

The manufacturing process of handling preregs deposited with thermoplastic nanofibers via room temperature electrospinning was carried out on aerospace grade pre-impregnated CFRP composite plies. Though the nanofibers were ultra-thin and low-density, apparent improvement (up to 20%) in fracture toughness was achieved.

Fracture toughness tests showed an increase of 18% and 17% in modes I and II, respectively. High variability was observed in some test data which is attributed to the low number of tested specimens (3-5 specimens per test category).

The TNFs had low concentration of 0.2 g/m<sup>2</sup>, which would give a total of 3.2 g/m<sup>2</sup> on an impact specimen (100mm × 150mm), significantly lower than the state-of-the-arts in the literature, thus almost with zero weight penalty (theoretically 0.5 g per specimen; less than 0.5% weight), which is one of the main advantage of this rapid toughening technology. The modified composite laminate had to be cured at 180°C under seven bar autoclave pressure, conditions at which the nylon doesn't keep its mechanical properties. It is therefore concluded that the TNFs can behave as nylon toughening interleaves for rapid laminate manufacturing.



## Acknowledgments

The authors would like to acknowledge the UK EPSRC funded projects, STRAINcomp (Ref. No. EP/R016828/1) and CAMREG (Ref. No. EP/P007805/1). The authors would also like to thank supports from Munro Technology Ltd, and Jim Hurley and Ben Hopper at the Enhanced Composites & Structures Centre at Cranfield University.

## References

- [1] J. Schoen, T. Nyman, A. Blom, H. Ansell, A numerical and experimental investigation of delamination behaviour in the DCB specimen, *Composites Science and Technology* 60(2) (2000) 173-184.
- [2] Y. Tang, L. Ye, Z. Zhang, K. Friedrich, Interlaminar fracture toughness and CAI strength of fibre-reinforced composites with nanoparticles—A review, *Composites Science and Technology* 86 (2013) 26-37.
- [3] N. Sela, O. Ishai, Interlaminar fracture toughness and toughening of laminated composite materials: a review, *Composites* 20(5) (1989) 423-435.
- [4] C. Lopes, O. Seresta, Y. Coquet, Z. Gürdal, P. Camanho, B. Thuis, Low-velocity impact damage on dispersed stacking sequence laminates. Part I: Experiments, *Composites Science and Technology* 69(7-8) (2009) 926-936.
- [5] R. Olsson, Experimental validation of delamination criterion for small mass impact, 16th International Conference on Composite Materials, 2007.
- [6] H. Zabala, L. Aretxabaleta, G. Castillo, J. Urien, J. Aurrekoetxea, Impact velocity effect on the delamination of woven carbon–epoxy plates subjected to low-velocity equienergetic impact loads, *Composites Science and Technology* 94 (2014) 48-53.
- [7] R. Bhanushali, D. Ayre, H. Yazdani Nezhad, Tensile response of adhesively bonded composite-to-composite single-lap joints in the presence of bond deficiency, (2017).
- [8] H.Y. Nezhad, F. Merwick, R. Frizzell, C. McCarthy, Numerical analysis of low-velocity rigid-body impact response of composite panels, *International journal of crashworthiness* 20(1) (2015) 27-43.
- [9] H.Y. Nezhad, Y. Zhao, P.D. Liddel, V. Marchante, R. Roy, A novel process-linked assembly failure model for adhesively bonded composite structures, *CIRP Annals* 66(1) (2017) 29-32.
- [10] H. Yazdani Nezhad, A. Auffray, C. McCarthy, R. O'Higgins, Impact damage response of carbon fibre-reinforced aerospace composite panels, ICCM, 2015.
- [11] E. Fuoss, P.V. Straznicky, C. Poon, Effects of stacking sequence on the impact resistance in composite laminates—Part 1: parametric study, *Composite structures* 41(1) (1998) 67-77.
- [12] X. Zhuang, K. Jia, B. Cheng, K. Guan, W. Kang, Y. Ren, Preparation of polyacrylonitrile nanofibers by solution blowing process, *Journal of Engineered Fibers and Fabrics* 8(1) (2013) 88-93.
- [13] P. Akangah, S. Lingaiah, K. Shivakumar, Effect of Nylon-66 nano-fiber interleaving on impact damage resistance of epoxy/carbon fiber composite laminates, *Composite Structures* 92(6) (2010) 1432-1439.
- [14] X.-F. Wu, Fracture of advanced polymer composites with nanofiber reinforced interfaces, 2003.
- [15] K. Shivakumar, S. Lingaiah, H. Chen, P. Akangah, G. Swaminathan, L. Russell, Polymer nanofabric interleaved composite laminates, *AIAA journal* 47(7) (2009) 1723-1729.
- [16] R. Palazzetti, A. Zucchelli, C. Gualandi, M. Focarete, L. Donati, G. Minak, S. Ramakrishna, Influence of electrospun Nylon 6, 6 nanofibrous mats on the interlaminar properties of Gr–epoxy composite laminates, *Composite structures* 94(2) (2012) 571-579.

- [17] H. Saghafi, R. Palazzetti, A. Zucchelli, G. Minak, Impact response of glass/epoxy laminate interleaved with nanofibrous mats, *Engineering Solid Mechanics* 1(3) (2013) 85-90.
- [18] G. Giuliese, R. Palazzetti, F. Moroni, A. Zucchelli, A. Pironi, Cohesive zone modelling of delamination response of a composite laminate with interleaved nylon 6, 6 nanofibres, *Composites Part B: Engineering* 78 (2015) 384-392.
- [19] H. Saghafi, A. Zucchelli, R. Palazzetti, G. Minak, The effect of interleaved composite nanofibrous mats on delamination behavior of polymeric composite materials, *Composite Structures* 109 (2014) 41-47.
- [20] T. Brugo, G. Minak, A. Zucchelli, H. Saghafi, M. Fotouhi, An investigation on the fatigue based delamination of woven carbon-epoxy composite laminates reinforced with polyamide nanofibers, *Procedia Engineering* 109 (2015) 65-72.
- [21] T. Brugo, G. Minak, A. Zucchelli, X. Yan, J. Belcari, H. Saghafi, R. Palazzetti, Study on Mode I fatigue behaviour of Nylon 6, 6 nanoreinforced CFRP laminates, *Composite Structures* 164 (2017) 51-57.
- [22] R. Palazzetti, A. Zucchelli, I. Trendafilova, The self-reinforcing effect of Nylon 6, 6 nanofibres on CFRP laminates subjected to low velocity impact, *Composite Structures* 106 (2013) 661-671.
- [23] T. Brugo, R. Palazzetti, The effect of thickness of Nylon 6, 6 nanofibrous mat on Modes I-II fracture mechanics of UD and woven composite laminates, *Composite Structures* 154 (2016) 172-178.
- [24] J. Zhang, T. Yang, T. Lin, C.H. Wang, Phase morphology of nanofibre interlayers: critical factor for toughening carbon/epoxy composites, *Composites science and technology* 72(2) (2012) 256-262.
- [25] HexPly® M21 curing epoxy matrix - Product datasheet, Hexcel corporation., 2015.
- [26] S. Heimbs, T. Bergmann, High-velocity impact behaviour of prestressed composite plates under bird strike loading, *International Journal of Aerospace Engineering* 2012 (2012).
- [27] D.-. ASTM, Standard test method for mode I interlaminar fracture toughness of unidirectional fiber-reinforced polymer matrix composites, *ASTM Internat.*, 2007.
- [28] D.D.M. ASTM, Standard Test Method for Determination of the Mode II Interlaminar Fracture Toughness of Unidirectional Fiber-Reinforced Polymer Matrix Composites, *ASTM Standard*, 2014.
- [29] N. Athanasopoulos, A. Kotzakolios, P. Irving, V. Kostopoulos, Numerical modelling and experimental verification of the low velocity impact response of composite panels made by a new toughened aeronautic resin.
- [30] D.-. ASTM Standard Test Methods for Flexural Properties of Unreinforced and Reinforced Plastics and Electrical Insulating Materials, *ASTM*, 2017.